ISIJ International, Vol. 45 (2005), No. 3, pp. 380–387

Ferrite/Pearlite Band Prevention in Dual Phase and TRIP Steels: Model Development

W. XU, P. E. J. RIVERA-DÍAZ-DEL-CASTILLO[1)] and S. van der ZWAAG[1)]

Visiting Scholar from the Department of Modern Mechanics, Key Laboratory of Mechanical Behaviour and Design of Materials, University of Science and Technology of China, Hefei, Anhui, PR China, 230027.
1) Faculty of Aerospace Engineering, Delft University of Technology, Kluyverweg 1, 2629 HS Delft, The Netherlands.
E-mail: p.rivera@lr.tudelft.nl

(*Received on August 27, 2004; accepted in final form on January 14, 2005*)

A model for predicting the conditions for ferrite/pearlite band prevention in dual phase and TRIP steels has been developed. The competition between processing parameters such as the austenitisation time and temperature, the transformation temperature and microchemical segregation wavelength is explored. The effects of alloy composition in the tendency to form ferrite/pearlite bands are quantified. A simple formula combining processing parameters and compositions for describing band formation is presented. The calculations show that the most prominent factor for preventing banding is the control of the microchemical wavelength. In addition to C and Mn, Al and Si concentrations have shown to play a smaller but significant role in band formation behaviour.

KEY WORDS: segregation; banding; ferrite; pearlite; microstructural homogeneity; kinetics; phase transformations; diffusion; nucleation; solidification.

1. Introduction

The prevention of ferrite/pearlite banding in high strength steels is an important technological boundary condition to allow utilising the full potential of their mechanical properties. The mechanism of formation of banded structures has been reviewed by Bastein,[1)] who determined the relationship between the formation of dendrites in solidification and microchemical inhomogeneity. The nucleation of new phases occurs in composition distinctive regions leading to the ferrite/pearlite band formation when cooling from the austenitic region. Kirkaldy, Von Destinon-Fortsmann and Brigham[2)] further established a quantitative relationship between the heat treatment scheme and the microchemical wavelength λ, defined as the average distance between parallel bands of composition. Grange[3)] observed that austenitisation at temperatures over 1 590 K prevents ferrite/pearlite band formation in Fe–C–Mn–Si steels. More recently, Thompson and Howell[4)] related austenite grain size to band prevention, whereas Großterlinden *et al.*[5)] spotted Mn segregation as the determining factor in banding. There is therefore extensive literature reporting the competing factors leading to banding and its prevention,[6)] however the concepts are formulated such that quantitative rules are hard to distil.

A predictive model quantifying the effects of themromechanical treatment on band prevention may be of great use. One of these models has been developed by Offerman *et al.*[7)] for a hot rolled medium carbon steel. In this model the ferrite nucleation rates are calculated in composition distinctive regions of Mn, Si and Cr; and based on experimental data, it is postulated that when the difference in ferrite nucleation rates exceeds 6–8%, ferrite/pearlite banding occurs. Rivera *et al.*[8)] further developed this concept by combining it with the calculation of segregation due to solidification employing a thermochemical database,[9)] with the theory of diffusion[10)] and with the classical nucleation theory.[11)] Their results were consistent with the experimentally observed conditions for ferrite/pearlite band prevention reported for a number of steel grades in the literature.[3,7)] The influence of processing parameters in banding was calculated for a number of industrial steel grades by introducing "band prevention plots"[12,13)] as a means to relate the austenitisation temperature (AT) and the transformation temperature (TT) with the austenitisation time (At) and microchemical wavelength (λ), an example of which is shown in **Fig. 1**.

Although the band prevention plots provide direct information for determining the processing conditions for preventing ferrite/pearlite band formation for a given segregation wave length, separate plots are required for each steel grade. The calculation time required for determining one of such plots is significant as its determination lays on solving the diffusion equation employing the finite differences method in the multicomponent scenario. The present work is aimed at quantitatively determining the effect of the general processing conditions required for preventing banding in high strength steels of varied composition. Furthermore, it is intended to condense the outcome of such elaborated calculations in a simple analytical equation of use to industry. The experimental validation of the model will be presented in the companion paper.[14)]

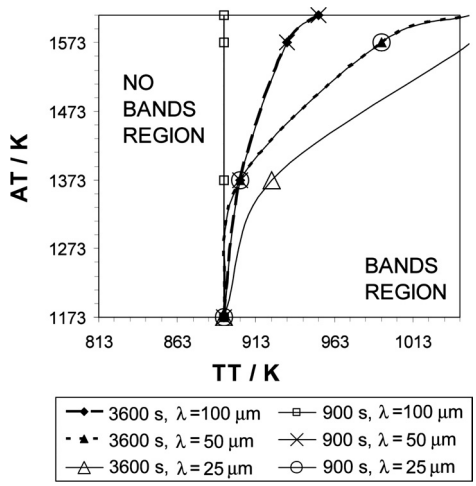

Fig. 1. Fe–0.1C–1.5Mn–0.14Si–0.8Cr (wt%) band prevention plot for the indicated austenitisation times and microchemical wavelengths.[12,13]

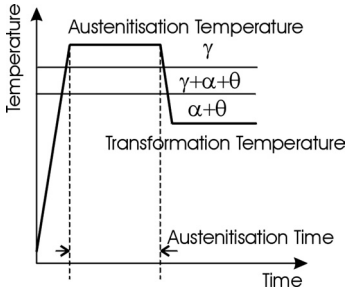

Fig. 2. Schematic representation of the heat treatment.

2. Model for Ferrite/Pearlite Band Prevention

The computer model combines the effects of solute segregation due to solidification, the diffusion of the segregated components during homogenisation and the nucleation of ferrite in regions possessing different concentration values during controlled cooling after hot rolling. The diffusion is assumed to occur in the austenitic field γ, and the transformation either in the three phase region $\gamma+\alpha+\theta$ or in the two phase region $\gamma+\theta$ (where α stands for ferrite and for θ stands for cementite), as shown schematically in **Fig. 2**.

2.1. Solidification and Solute Segregation

The first phenomenon leading to ferrite/pearlite banding that takes place in alloy production is solidification. At this stage, the primary and secondary dendrite arms advance towards fresh liquid regions. This causes an inhomogeneous solute distribution in the dendrite, where its centre contains the low carbon content that characterises the liquid$\rightarrow\delta$-ferrite reaction at the alloy concentration. The dendrite edges impinge with each other in the last stages of solidification, requiring that such interfaces be characterised by the high carbon concentration of the eutectic point. Therefore, the liquid$\rightarrow\delta$-ferrite composition and eutectic reaction composition provide the extreme composition values to be homogenised in the high temperature austenitisation treatment. These were obtained for a variety of steels from a thermochemical database.[9] The procedure employed for each studied alloy grade was to reduce the temperature from the liquid field to the eutectic temperature. The δ-ferrite composition and the composition of the last liquid in equilibrium were assumed to be the initial segregation values present, which will approach the average alloy concentration as homogenisation proceeds.[8] Reduced segregation values obtained from non-equilibrium solidification processes may be incorporated in the model through assuming an increased austenitisation time value. However, the equilibrium composition values that are assumed capture very well the expected compositional variations across the dendrites as a function of alloy composition. Moreover, the major responsible for the homogenisation of segregated regions is the austenitisation process to be described next.

2.2. High Temperature Homogenisation

The alloy is homogenised in the austenitic region (Fig. 2). The evolution of the segregated solutes resulting form solidification is numerically described by solving Fick's second law in the multicomponent scenario. Kirkaldy and Young[10] have expressed the solute kinetics with a finite differences algorithm

$$C_k^{i+1,j}=C_k^{i,j}+\frac{\Delta t}{(\Delta x)^2}\times\sum_{p=1}^{m}[(D_{kp}^{j+1}-D_{kp}^{j})(C_p^{i,j+1}-C_p^{i,j}) +(D_{kp}^{j})(C_p^{i,j+1}-2C_p^{i,j}+C_p^{i,j-1})] \quad \text{.....(1)}$$

where $C_k^{i+1,j}$ is the k concentration at time $i+1$ in node j, Δt is the size of the time interval, Δx is the distance between nodes and $D_{kp}^{j+1}=\partial D_k^{j+1}/\partial C_p$ is the variation of k component diffusion coefficient at node $j+1$, D_k^{j+1}, with the p component concentration, C_p.

In the present calculations, the number of nodes was taken as $j=0, 1, \ldots, 50$. The presence of isoconcentrate bands was expressed as the boundary condition

$$C_k^{i,j-1}=C_k^{i,j+1} \quad \text{.....(2)}$$

for $j=0$, 50.

The carbon interdiffusion coefficients are approximated as[15]

$$D_{Ck}=\frac{\partial\mu_C/\partial N_k}{\partial\mu_C/\partial N_C}D_{CC} \quad \text{.....(3)}$$

where subindex C stands for carbon and k for a substitutional solute, and μ and N stand for chemical potential and mole number, respectively.

The carbon diffusion coefficient in austenite, D_{CC}, is calculated from[16]

$$D_{CC}=4.53\times10^{-7}\cdot(1+Y_C(1-Y_C)\cdot 8\,339.9T^{-1}) \times\exp\{-(T^{-1}-2.221\times10^{-4})(17\,767-26\,436Y_C)] \quad \text{.....(4)}$$

where T is the austenite temperature in K, and $Y_C=C_C/(1-C_C)$ is the site fraction of carbon in the interstitial sublattice. D_{CC} is in $m^2\,s^{-1}$.

The diffusion coefficients for the substitutional solutes were calculated from

$$D_{kk}=D_{k0}\exp\{-Q_k/RT\} \quad \text{.....(5)}$$

where R and T are the universal gas constant and austeniti-

sation temperature, respectively. D_{k0} and Q_k are the k component diffusivity pre-exponential factor and activation energy for diffusion.

The updating of solute composition across microchemical bands with Eq. (1), is carried out by approximating the initial extreme values present at the centre and edge of the dendrites by a second order polynomial function. The details of this approximation can be found elsewhere.[8)]

2.3. Transformation

The application of Eq. (1) for each alloy component provides the demise of the microchemical composition bands originally present in the austenitic state. Recent experimental work from Offerman *et al.* indicates that the presence of ferrite/pearlite bands can be determined when the difference r in ferrite nucleation rates across the microchemical bands exceeds a threshold value of $r \approx 0.06$–0.08[7,17)] and when carbon can diffuse in austenite over an appropriate distance consistent with pearlite formation along the microchemical waves.[7)] A value of $r=0$ implies a uniform rate of ferrite nucleation across the microchemical bands. A necessary condition for an alloy to possess ferrite/pearlite banding is the ferrite nucleation at approximately parallel preferential sites, which are compositionally dependent. The parameter r captures such effect. Consistent with previous experimental work, in the present model assumes that bands form for $r>0.07$. Such a difference in nucleation rates may be calculated as[7)]

$$r = \frac{(dN/dt)_{N1} - (dN/dt)_{N2}}{(dN/dt)_{N1}} = 1 - \exp\left\{\frac{\tau}{k_B T}(\Delta G^*_{N1} - \Delta G^*_{N2})\right\} \quad \text{.....(6)}$$

where $(dN/dt)_{N1}$ and $(dN/dt)_{N2}$ are the changes in nucleation rate in nodes $N1$ and $N2$, which are selected to maximise r; k_B is the Boltzmann's constant, ΔG^*_{N2} and ΔG^*_{N1} are the energy barriers for α nucleation at the compositions that characterise nodes $N1$ and $N2$, respectively.

Referring to Eq. (6), τ is a scaling parameter which was taken as 0.0015 for all alloys. The need of this parameter has been discussed elsewhere.[18–21)] The effects of composition across the microchemical bands are captured by obtaining the energy barriers

$$\Delta G^* = \frac{4(z_2\gamma_{\alpha\gamma} - z_1\gamma_{\gamma\gamma})^3}{27 z_3 \Delta G_v^2} \quad \text{.....(7)}$$

where z_1, z_2 and z_3 are geometrical parameters that depend on the type of nucleation site in the austenite grain,[7)] $\gamma_{\alpha\gamma}=0.6\ \mathrm{J\,m^{-2}}$ and $\gamma_{\gamma\gamma}=0.85\ \mathrm{J\,m^{-2}}$ are the interfacial energies per unit area of the α/γ interface and γ/γ grain boundary[7)] and ΔG_v is the driving force for volume nucleation. ΔG_v was obtained from

$$\Delta G_m = C_k^{\alpha\gamma}\cdot\mu_k^{1-n\gamma} - C_k^{\alpha\gamma}\cdot\mu_k = C_k^{\alpha\gamma}\cdot(\mu_k^{\gamma} - \mu_k) \quad \text{.....(8)}$$

which represents a dot product. ΔG_v was approximated by dividing ΔG_m over the ferrite molar volume. Therefore, ΔG_v captures the influences of all the alloy components, and the original simplification of assuming the steel to be a system of the type Fe–C–X (where X is a substitutional solute such as Mn) was removed. Thus, all the chemical potential cross effects are accounted.

Table 1. Composition of studied grades.

GRADE	C wt%	Si wt%	Mn wt%	Al wt%	Cr wt%	Fe wt%
DP1	0.1356	0.1319	1.4852	0.03	0.3723	balance
DP2	0.065	0.11	1.41	0.051	0.741	balance
DP3	0.15	0.2	1.9	0.03	0.2	balance
TRIP1	0.2	1.65	1.65	0.038	--	balance
TRIP2	0.2	0.3	1.5	1	--	balance
TRIP3	0.2	1.5	1.5	--	--	balance

Table 2. Diffusivity and activation energy for diffusion employed in calculations.

component k	Temperature range / K	D_{k0} / 10^{-4} m^2 s^{-1}	Q_k / 10^3 J mol^{-1}	Reference
Si	1173-1613	7.0	286	22)
Mn	1173-1573	0.178	264	23-25)
Mn	1573-1613	0.486	276	26)
Al	1173-1613	3.5	286	22)
Cr	1173-1373	0.21	300	27)
Cr	1373-1613	10.8	292	28)

3. Application of the Model to Dual Phase and TRIP Steels

The outlined model was applied to a variety of high strength dual phase and TRIP steels which composition is listed in **Table 1**.

Apart from the chemical potentials, the Gibbs energies for α formation and the initial segregation values obtained form MTData, the other input parameters for the present model are the diffusivity and activation energy for diffusion. The employed literature values are listed in **Table 2**.

The progress in solute homogenisation was obtained from Eq. (1). This microchemical component variation with time is an input to obtaining the driving force for α formation (Eq. (8)), and the variation of its nucleation rates (Eq. (6)). One example for solute homogenisation is given in **Fig. 3** for DP1 austenitised at 1 473 K and $\lambda=50\ \mu$m for the indicated times. Figures 3(a)–3(e) show the nodal progress in solute concentration. These figures indicate that the progress towards homogenisation depends on the diffusivity of the concerned species. C will reach a homogenous concentration within the first 10 s of heat treatment. Conversely, Mn will not homogenise even after about 3 600 s of heat treatment. Those effects derive from the diffusivity of C being several orders of magnitude larger than those from the substitutional components. The homogenisation behaviours of the rest of the solutes lay in between C and Mn. The shifting towards an equilibrium composition is highly dependent on the wavelength and the temperature, as it will be assessed next.

Nodes $N1$ and $N2$ are those that maximise the difference ΔG_m and hence r. They were chosen by the computer program in every time step progressing towards homogenisation. It was seen that nodes $N1$ and $N2$ usually correspond-

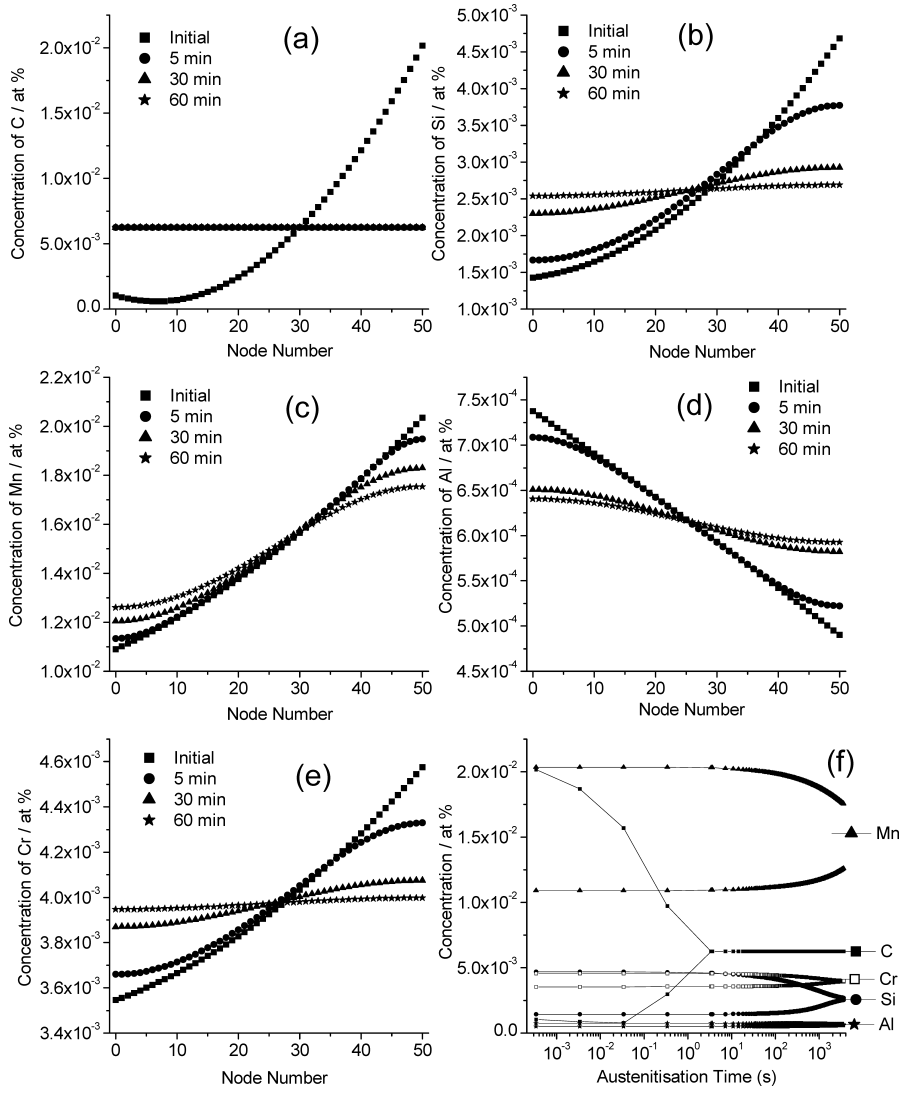

Fig. 3. Progress in nodal microchemical concentration of DP1 across microchemical bands for 1 473 K and $\lambda = 50\ \mu$m.

ed to nodes 0 and 50, indicating that the extreme compositions are those that maximise the ferrite nucleation driving force within the MTData typical accuracy range of 10^{-6} in solute atom fraction. The progress in the concentration of nodes 0 and 50 is shown in Fig. 3(f).

Band prevention plots were generated for all steel grades shown in Table 1 for a variation of the microchemical wavelength through further rolling at an austenitisation time of 3 600 s (**Fig. 4**) and through the variation of the austenitisation time by increasing the homogenisation time for a microchemical wavelength of 25 μm (**Fig. 5**). These figures indicate that the non-desirable regions where ferrite/pearlite bands will be present are on the left and top of each figure, *i.e.* for high transformation temperatures and low austenitisation temperatures.[8,13] They show a limiting minimum value for the transformation temperature. Thus, a critical minimisation transformation temperature can be achieved irrespective of microchemical wavelength and austenitisation time for low values of austenitisation temperature. It is, however, preferable to have a value for the transformation temperature as large as possible, such that the kinetics of ferrite formation can be controlled at the cooling rate required by the aimed microstructure. Figures 4 and 5 also indicate that the limiting value for the transformation temperature is composition dependent.

Figures 4 and 5 are an aid in determining the processing conditions for preventing the formation of ferrite/pearlite bands. A decrease in the microchemical wavelength through further rolling or an increase in austenitisation time allows lower austenitisation temperatures for a desired transformation temperature (Figs. 4 and 5). This has already been pointed out elsewhere.[8,13] The influence of the wavelength and alloy composition remains, however, to be explored.

The symmetry of Figs. 4 and 5 suggests the possibility to approximate the transformation temperature with an analytical expression. An Arrhenius type of approximation is suggested due to the nature of the thermally activated process. Furthermore, a dependence of the type At/λ^2 is suggested by exploring Eq. (1). Several approximations were tried, and the best fit was obtained with

$$TT = a + 0.06\,\frac{At}{\lambda^2}\,e^{b/AT} \quad \text{.....(9)}$$

$$a = 997 + 1\,665c_{\mathrm{C}} - 5c_{\mathrm{Si}} - 43c_{\mathrm{Mn}} - 18c_{\mathrm{Al}} \quad \text{.....(10)}$$

$$b = -33\,139 - 2\,244c_{\mathrm{C}} + 201c_{\mathrm{Si}} + 134c_{\mathrm{Mn}} + 1\,286c_{\mathrm{Al}} \quad \text{...(11)}$$

where TT and AT are the transformation and austenitisation

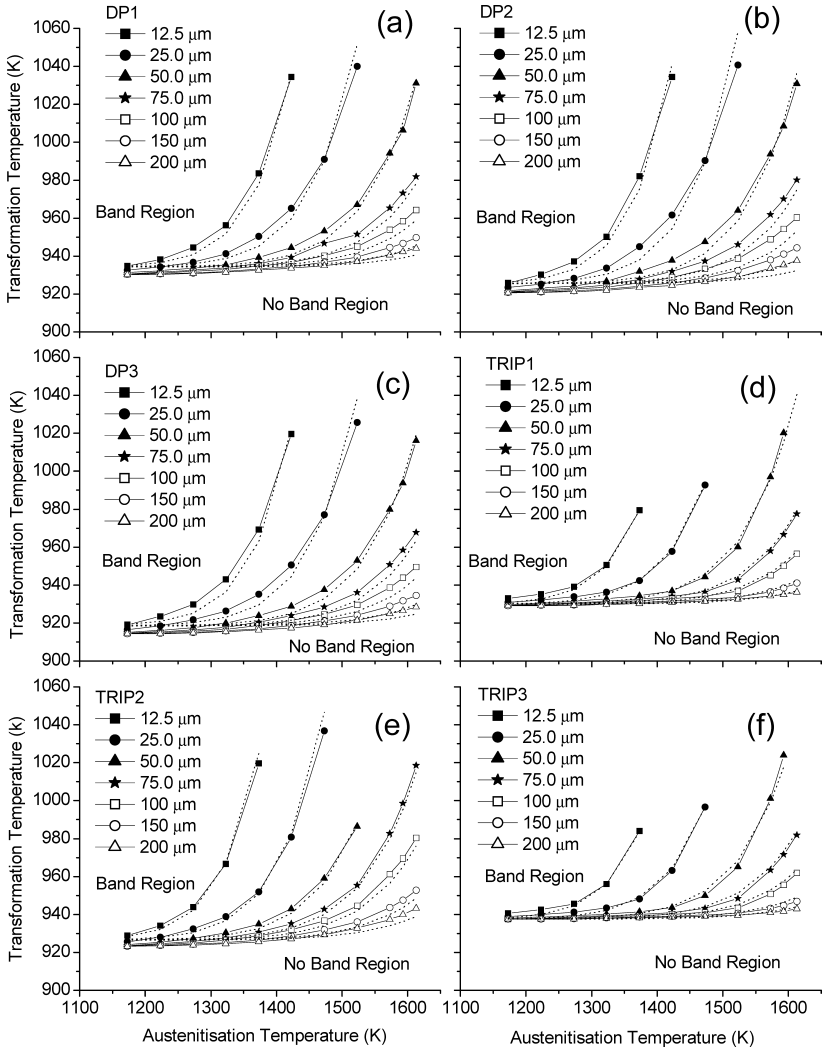

Fig. 4. Effect of microchemical wavelength variation in band prevention plots for the studied grades at an austenitisation time of 3 600 s. The solid lines are obtained from the numerical computations and the dotted lines result from employing Eq. (9).

temperatures in K, λ is the microchemical wavelength expressed in metres and At is the austenitisation time in seconds. The coefficients a and b are expressed in K, they depend on the alloy compositions of C, Si, Mn and Al expressed in weight fraction, namely c_C, c_{Si}, c_{Mn}, c_{Al}. It was observed that the application of Eq. (9) fitted extremely well all the numerical results shown in Figs. 4 and 5 with the expressions C and A shown above. C determines the slope of the band prevention plots and A depends on the point where Figs. 4 and 5 converge. The application of Eq. (9) is shown in the dotted lines adjacent to each band prevention plot in those figures.

Equation (9) provides a new framework for exploring the influences of the composition and the microchemical wavelength.

3.1. Composition

Equations (10) and (11) indicate dependence of banding behaviour on Al and Si composition in addition to the influence of Mn and C that has been spotted in previous works.[4,6] This dependence is of a lower degree and was corroborated by a number of computer experiments set in alloys of compositions around those shown in Table 1. If those are taken as reference compositions, and the new alloy compositions are normalised to them, the transformation temperature was obtained employing the numerical model for an austenitisation temperature of 1 373 K, an austenitisation time of 3 600 s and a microchemical wavelength of 75 μm. **Figure 6** shows the results of those calculations, indicating that Mn is the major component influencing banding followed by C. This is in agreement with previous experimental work,[4-6] however Al and Si play also a role in the transformation behaviour.

3.2. Microchemical Wavelength

The variation of transformation temperature with microchemical wavelength for an austenitisation temperature of 1 473 K is shown in **Fig. 7**. In this figure, the region in which ferrite/pearlite bands are expected to form is on the top right, *i.e.* for large microchemical wavelengths (low degrees of rolling) and high transformation temperatures. The application of Eq. (9) to the different steel grades is indicated by the dotted line, reproducing with remarkable accuracy the results of the numerical computations. It is worth noting that band prevention is most sensitive to microchemical wavelength values under 20 μm. This corresponds to

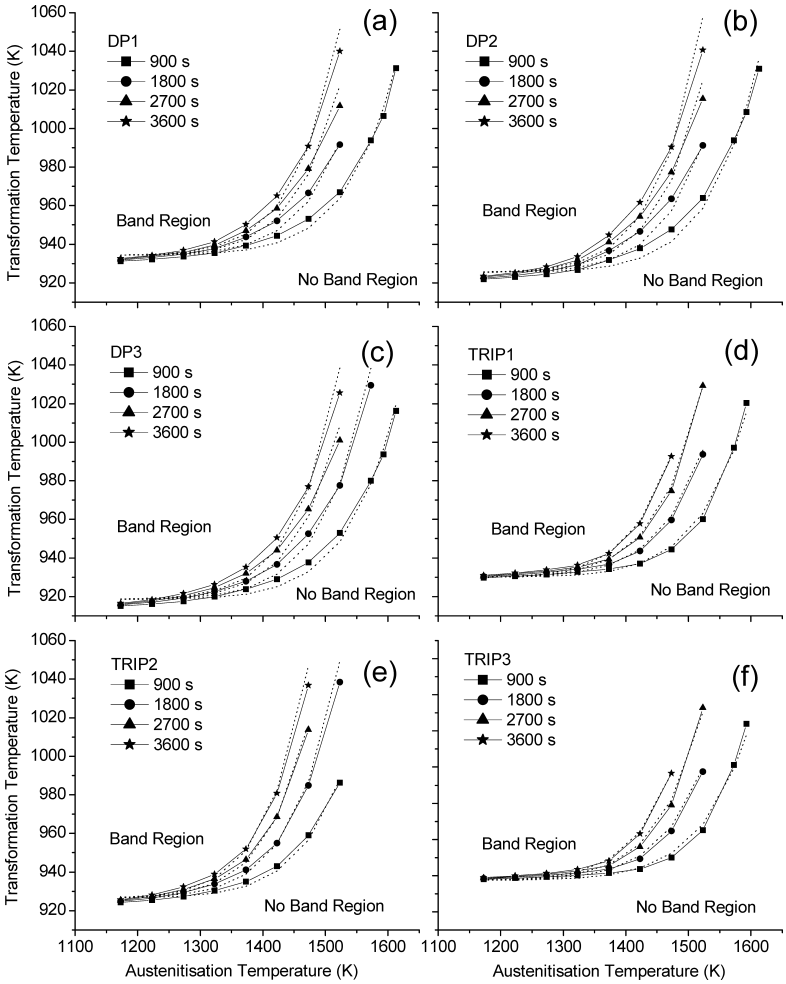

Fig. 5. Effect of austenitisation time variation in band prevention plots for the studied grades with a microchemical wavelength of 25 μm. The solid lines are obtained from the numerical computations and the dotted lines result from employing Eq. (9).

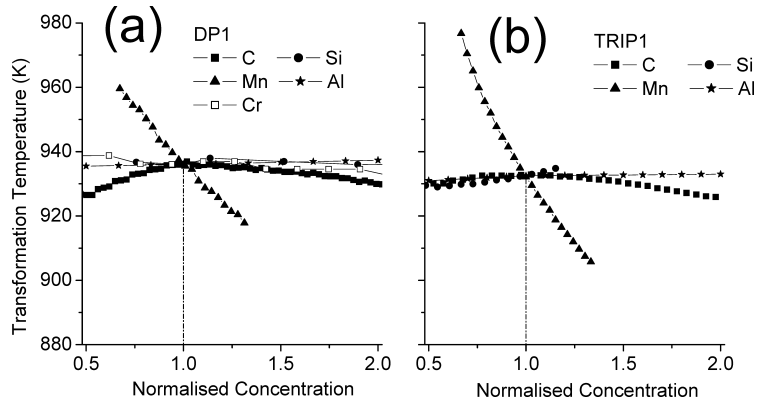

Fig. 6. Variation of transformation temperature for concentrations normalised to the grades given in Table 1. Austenitisation temperature of 1 373 K and an austenitisation time of 3 600 s. The microchemical wavelength was taken as 75 μm.

the case of many industrial steel grades, where different sections of the sheet may possess a variation in microchemical wavelength. The application of Eq. (9) should thus account for such wavelength dispersions.

3.3 Applicability of the Model

Equations (9) and (10) were derived combining semi-empirical methods with thermokinetic approaches. The accuracy of their application to a large number of experimental alloys possessing the compositions indicated in Table 1 will be explored in the companion paper.[14] The accuracy of Eq. (9) may be tested by applying it to the band prevention scheme reported by Grange[3] for alloy grades G1 and G2 shown in **Table 3**. It was experimentally found that ferrite/pearlite bands may be prevented in grades G1 and G2 by applying a 600 s heat treatment between 1 588 and 1 618 K followed by air cooling. The use of Eq. (9) will require that the value of the transformation temperature

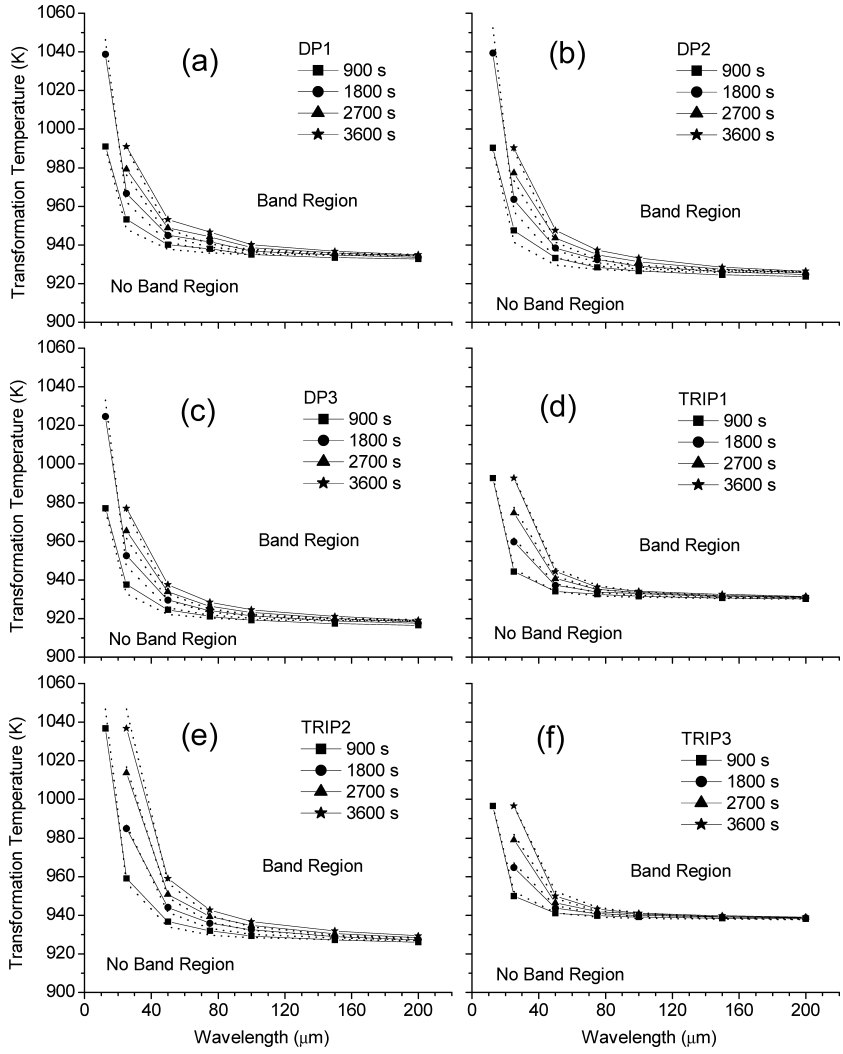

Fig. 7. Variation of transformation temperature with wavelength for different austenitisation times and an austenitisation temperature of 1 473 K. The solid lines are obtained from the numerical computations and the dotted line result from employing Eq. (9).

Table 3. Composition of G1 and G2 alloys studied by Grange.

Grade	C wt%	Si wt%	Mn wt%	P wt%	S wt%	Fe wt%
G1	0.25	0.005	1.5	0.015	0.006	balance
G2	0.25	0.22	1.5	0.015	0.019	balance

Table 4. Austenitisation temperature required for preventing ferrite/pearlite band formation for different wavelengths.

Grade	Ac3 (K)	AT (K)	
		λ=15 μm	λ=19 μm
G1	1059	1587	1623
G2	1065	1590	1626

$TT \geq$Ae3, implying that, on cooling form the austenitic region, no significant difference in the ferrite nucleation rate will cause banding. The value for the austenitisation temperature was calculated from Eq. (9) for wavelengths between 15 and 19 μm (corresponding to those reported) and an austenitisation time of 600 s. The results are shown in **Table 4**, indicating a required austenitisation temperature of 1 587 to 1 626, in close agreement with the range experimentally obtained by Grange.[3)]

4. Summary and Conclusions

A simple algebraic expression for determining the processing conditions for ferrite/pearlite band prevention in high strength steels is provided. The equation relates the austenitisation time and temperature, microchemical wavelength, alloy composition and transformation temperature. The equation incorporates the alloying effects of Al and Si in addition to those of Mn and C, and it was demonstrated that the segregation of other components plays a negligible effect in the prevention of the formation of ferrite/pearlite bands. The equation provides a simple and accurate methodology to obtaining the processing conditions for band prevention without the use of complex thermochemcial databases and numerical methods. Microchemical wavelength was shown to play a dominant role in banding for values under 20 μm.

Acknowledgements

The authors are grateful for financial support from the ECSC through programme "Suppression of Banded Structure and Refinement of the Microstructure of High Strength Cold Rolled Steels by Optimisation of Hot Rolling and Cold Rolling Path". Mr W. Xu is grateful to the Nuffic

for the provision of a Huygens scholarship.

REFERENCES

1) P. G. Bastien: *J. Iron Steel Inst.*, (1957), 281.
2) J. S. Kirkaldy, J. Von Destinon-Fortsmann and R. J. Brigham: *Can. Metall. Q.*, **1** (1962), 59.
3) R. A. Grange: *Metall. Trans.*, **2** (1971), 417.
4) S. W. Thompson and P. R. Howell: *Mater. Sci. Technol.*, **8** (1992), 777.
5) R. Großterlinden, R. Kawalla, U. Lotter and H. Pircher: *Steel Res.*, **63** (1992), 331.
6) J. D. Verhoeven: *J. Mater. Eng. Perform.*, **9** (2000), 286.
7) S. E. Offerman, N. H. van Dijk, M. T. Rekveldt, J. Sietsma and S. van der Zwaag: *Mater. Sci. Technol.*, **18** (2002), 297.
8) P. E. J. Rivera Diaz del Castillo, J. Sietsma and S. van der Zwaag: *Metall. Mater. Trans. A*, **35A** (2004), 425.
9) MTDATA: Metallurgical and Thermochemical Databank, National Physical Laboratory, Teddington, Middlesex, United Kingdom, (1995).
10) J. S. Kirkaldi and D. J. Young: Diffusion in the Condensed State, Institute of Materials, London, (1987).
11) J. W. Christian: The Theory of Transformations in Metals and Alloys, Part II, Pergamon, Oxford, (2002).
12) P. E. J. Rivera Díaz del Castillo and S. van der Zwaag: Proc. of the Sixth Int. Conf. for Micromechanics, Saradidis Publications, Patras, Greece, (2004), 261.
13) P. E. J. Rivera Díaz del Castillo and S. van der Zwaag: *Steel Res. Int.*, **75** (2004), No. 11, 711.
14) P. E. J. Rivera Díaz del Castillo and S. van der Zwaag: Private Communication.
15) L. C. Brown and J. S. Kirkaldi: *Trans. Metall. Soc. AIME*, **230** (1964), 223.
16) J. Ågren: *Scr. Metall.*, **20** (1986), 1507.
17) T. A. Kop, J. Sietsma and S. van der Zwaag: *Mater. Sci. Technol.*, **17** (2001), 1569.
18) S. E. Offerman, N. H. van Dijk, J. Sietsma, S. Grigull, E. M. Lauridsen, L. Marguiles, H. F. Poulsen, M. Th. Rekveldt and S. van der Zwaag: *Science*, **298** (2002), 1003.
19) M. Enomoto and H. I. Aaronson: *Metall. Trans. A*, **17A** (1986), 1385.
20) M. Enomoto, W. F. Lange III and H. I. Aaronson: *Metall. Trans. A*, **17A** (1986), 1399.
21) W. F. Lange III, M. Enomoto and H. I. Aaronson: *Metall. Trans. A*, **19A** (1988), 427.
22) J. Fridberg, L. E. Torndahl and M. Hillert: *Jernkontorets. Ann.*, **153** (1969), 263.
23) M. A. Krishtal and A. P. Mokrov: *Zaved. Lab.*, **33** (1967), 827.
24) T. Eguchi, Y. Iijima and K. Hirano: *Cryst. Lattice Defects*, **4** (1973), 265.
25) K. Nohara and K. Hirano: Suppl. to *Trans. Iron Steel Inst. Jpn.*, (1971), 1267.
26) C. Wells and R. F. Mehl: *Trans. AIME*, **145** (1941), 315.
27) A. M. Huntz, P. Guiraldenq, M. Aucouturier and P. Lacombe: *Mem. Sci. Rev. Met.*, **66** (1969), 85.
28) A. W. Bowen and G. M. Leak: *Metall. Trans.*, **1** (1970), 1695.